

Robust paramagnetism in $\text{Bi}_{2-x}\text{M}_x\text{Ru}_2\text{O}_7$ ($\text{M} = \text{Mn, Fe, Co, Ni, Cu}$) pyrochlore

M.K. Haas and R.J. Cava

*Department of Chemistry and Princeton Materials Institute,
Princeton University, Princeton, New Jersey 08540, USA*

M. Avdeev and J.D. Jorgensen

Argonne National Lab, Division of Materials Science, Argonne, IL 60439, USA

(Dated: June 2, 2021)

We report physical property characterization of $\text{Bi}_{2-x}\text{M}_x\text{Ru}_2\text{O}_7$ pyrochlores, including magnetic susceptibility, resistivity, and Seebeck coefficients. The solid solution exists up to $x=0.5$ for ($\text{M}=\text{Cu, Ni, Co}$) and up to $x=0.1$ for ($\text{M}=\text{Fe, Mn}$). None of the doped materials exhibit ferromagnetism or any localized ruthenium moment behavior. Instead we find the Ru-O and Bi-O sublattices to be essentially independent, with any magnetism resulting from the unpaired transition metal dopant spins. Cobalt substitution for bismuth results in localized Co^{2+} , and low temperature spin-glass transitions in several cases. Nickel moments on the pyrochlore lattice display properties intermediate to localized and itinerant. Finally, copper doping results in only an enhancement of the Pauli metallic density of states.

I. INTRODUCTION

Ruthenium oxide based perovskites are presently of great interest due to the range of magnetic and strongly correlated electronic behavior they exhibit, often breaching the limits of current condensed matter theory. Layered Sr_2RuO_4 , for example, is a superconductor at < 1 K,¹ and is postulated to have p -wave and spin-triplet pairing in the superconducting state.² Of particular interest is the delicate balance many ruthenate perovskites display between ferromagnetism and exotic electronic states. When superconducting Sr_2RuO_4 is doped by small amounts of nonmagnetic Ti^{4+} on the ruthenium site, there is a cross-over from superconductivity to short range ferromagnetic ordering.^{3,4} In the same structural system, $\text{Sr}_3\text{Ru}_2\text{O}_7$ shifts from a paramagnetic, strongly correlated Fermi-liquid to a ferromagnet under applied pressure.⁵ Also, at fields above 7T the compound undergoes a metamagnetic quantum transition to a high moment state.⁶ Finally, Ti^{4+} doping on the ruthenium site of CaRuO_3 induces ferromagnetism in what was originally a paramagnetic material.⁷

As much of the recent work focuses on perovskite based structures, the question follows as to whether the observed balance between itinerant and ferromagnetic behavior is characteristic of ruthenium oxides in general, or specific to perovskites. Therefore we have investigated another common oxide structure, the pyrochlore. The pyrochlore oxide $\text{Bi}_2\text{Ru}_2\text{O}_7$, which exhibits temperature independent Pauli paramagnetism and is weakly metallic, affords an excellent opportunity to test the generality of this balance.

Like the perovskite, the pyrochlore structure, $\text{A}_2\text{M}_2\text{O}_7$, contains a three dimensional network of corner-sharing MO_6 octahedra (fig. 1). In the perovskite these are regular MO_6 octahedra with $160\text{-}180^\circ$ M-O-M bonds, forming a three dimensional square net of metal atoms. However, in the pyrochlore the corner-sharing results in tetrahedrally related metal atoms, and coordination is

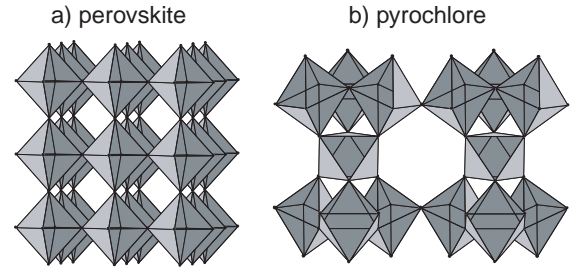


FIG. 1: View of RuO_6 network in a) perovskite along $\langle 100 \rangle$ and b) pyrochlore along $\langle 011 \rangle$.

such that the M-O-M bond angle must be $\sim 130^\circ$. The A cation in the pyrochlore occupies hexagonal channels along $\langle 011 \rangle$ and equivalent directions. Three dimensionally, the cations form an A_4O sublattice of corner sharing tetrahedra.

Previous experimental work has probed differences between $\text{Bi}_2\text{Ru}_2\text{O}_7$, $\text{Y}_2\text{Ru}_2\text{O}_7$, and $\text{Ln}_2\text{Ru}_2\text{O}_7$, the latter two being electronically insulating although isoelectronic to $\text{Bi}_2\text{Ru}_2\text{O}_7$.⁸ One proposed reason for the difference is the change in Ru-O-Ru angle with A cation size.^{9,10} It is also postulated that in the compounds $\text{Y}_2\text{Ru}_2\text{O}_7$ and $\text{Ln}_2\text{Ru}_2\text{O}_7$ the cation valence orbitals are energetically prohibited from contributing to Fermi level bonding, resulting in narrower localized bands.¹¹ Reports are conflicting as to whether bismuth s and p orbitals hybridize to some extent at the Fermi level, participating in conduction.^{12,13} Experimental work has followed the metal to insulator transition in several of these solid solutions.^{14,15} Here we report the properties of $\text{Bi}_{2-x}\text{M}_x\text{Ru}_2\text{O}_7$, $\text{M} = (\text{Mn, Fe, Co, Ni, Cu})$, observing that the first row transition metal d -orbitals are proximate to the energy of the Fermi level of $\text{Bi}_2\text{Ru}_2\text{O}_7$. Thus it is likely that the overall properties of these doped ma-

terials will be markedly different from those previously described in the literature.

II. EXPERIMENTAL

Suitable stoichiometric amounts of RuO_2 , Bi_2O_3 , Co_3O_4 , CuO , MnO_2 , Fe_2O_3 , and Ni_2O_3 were thoroughly ground in an agate mortar and pressed into pellets. RuO_2 was dried for 2 hours at 900°C before use. The pellets were successively heated in air at 750°C for 1 day, 900°C for 1 day, 950°C for 3 days, and 975°C for 1 day, with several intermediate grindings. Iron and nickel samples were heated for an additional day at 1020°C . Sample purity was monitored using room temperature powder X-ray diffraction employing $\text{Cu-K}\alpha$ radiation.

Magnetic properties and electrical resistivity were evaluated using a Quantum Design physical property measurement system (PPMS). For all samples, the susceptibility was measured from 300 to 5 K in an applied field of 1 T. Data were also collected from 2 to 30 K in a field of 1 T after zero-field cooling, to assess any low temperature magnetic transitions. Magnetic hysteresis loops were performed at 5 K in the range of -9 to 9 T, and the data were fit to the paramagnetic Brillouin function $M = NgJ\mu_B B(x)$ where $x = m\mu_0 H/k_B T$.¹⁶ Resistivity measurements were performed on sintered powder pellets, which were cut into bars of approximately $1.5 \times 1.5 \times 3.5$ mm, and measured with the standard 4-point AC method. Seebeck coefficient measurements employed a commercial apparatus (MMR technologies) within the temperature range 200-500 K.

III. RESULTS

Substitution of first row transition metals on the ruthenium site of $\text{Bi}_2\text{Ru}_2\text{O}_7$ was not possible within the synthetic conditions explored. The first row transition metals Mn, Fe, Co, Ni, and Cu instead substitute on the bismuth site of the pyrochlore. We report complete structural characterization of $\text{Bi}_{1.6}\text{Cu}_{0.4}\text{Ru}_2\text{O}_7$, $\text{Bi}_{1.6}\text{Co}_{0.4}\text{Ru}_2\text{O}_7$, and $\text{Bi}_2\text{Ru}_2\text{O}_7$ elsewhere,¹⁷ by refinement of neutron powder diffraction data. This type of substitution is not unprecedented, as synthesis of $\text{Bi}_{2-x}\text{Cu}_x\text{Ir}_{2-y}\text{Ru}_y\text{O}_7$ was reported, although the compound was not fully characterized.¹⁸

Figure 2 plots lattice parameters obtained from powder X-ray diffraction as a function of x for $\text{Bi}_{2-x}\text{M}_x\text{Ru}_2\text{O}_7$ ($\text{M}=\text{Cu},\text{Ni},\text{Co}$). To a first approximation the lattice parameters decrease linearly. This is consistent with the smaller radii of the first row transition metals in comparison to that of bismuth. For copper, nickel, and cobalt dopants, the solid solution exists up to $x=0.5$: at larger nominal concentrations the lattice parameters remain relatively constant. In several samples, RuO_2 is found as a very minor impurity. For example, the cobalt-doped sample with $x=0.4$, contains 0.5% RuO_2 by weight, as

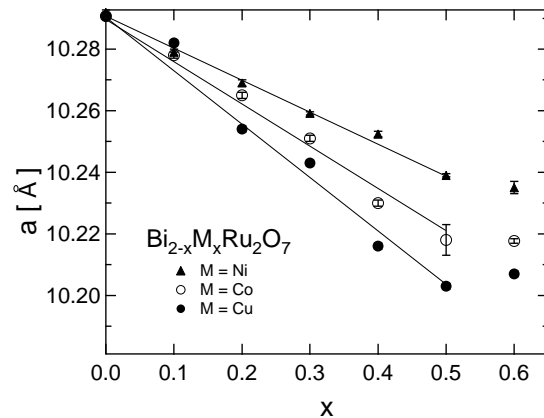


FIG. 2: Cubic lattice parameter, determined by powder x-ray diffraction, for $\text{Bi}_{2-x}\text{M}_x\text{Ru}_2\text{O}_7$ ($\text{M}=\text{Cu},\text{Ni},\text{Co}$) as a function of doping level.

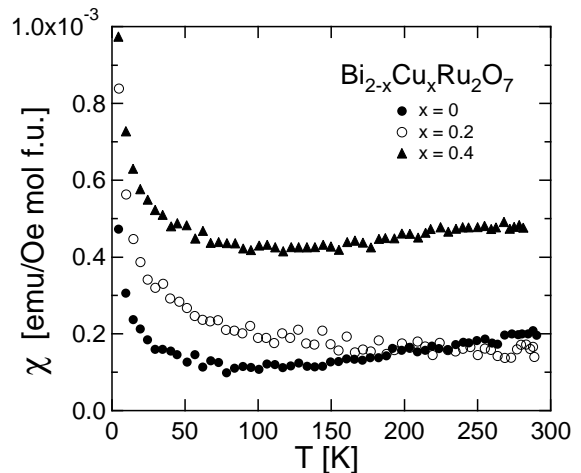


FIG. 3: Measured magnetic susceptibility as a function of temperature for $\text{Bi}_{2-x}\text{Cu}_x\text{Ru}_2\text{O}_7$.

determined by powder neutron diffraction refinement.¹⁷ As RuO_2 is non-magnetic, and the amount present is negligible, its presence will not affect physical property characterization. For iron and manganese-doped series the substitution limit is $x=0.1$, resulting in unit cells of $a=10.282(1)$ and $10.279(2)$ respectively.

A. $\text{Bi}_{2-x}\text{Cu}_x\text{Ru}_2\text{O}_7$

The magnetic susceptibility (χ) of $\text{Bi}_2\text{Ru}_2\text{O}_7$ between 300 and 5 K is plotted in figure 3. It is essentially temperature independent with a relatively small magnitude of 2×10^{-4} emu/Oe mol f.u., consistent with Pauli paramagnetism. Also plotted in figure 3 is the susceptibility of $\text{Bi}_{1.6}\text{Cu}_{0.4}\text{Ru}_2\text{O}_7$ and $\text{Bi}_{1.8}\text{Cu}_{0.2}\text{Ru}_2\text{O}_7$. It can be seen that $x=0.4$ copper-doping increases the magnitude of the temperature independent susceptibility by a

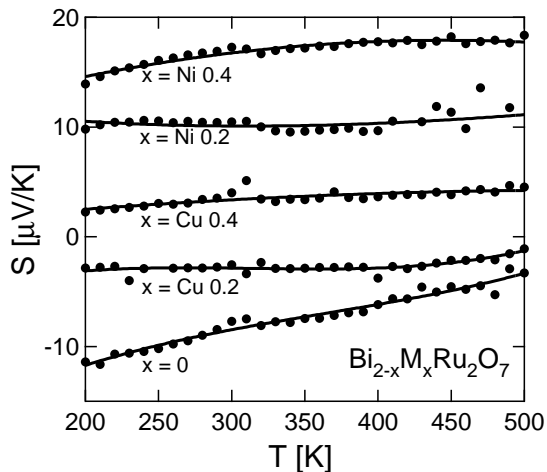


FIG. 4: Seebeck coefficients for $\text{Bi}_{2-x}\text{M}_x\text{Ru}_2\text{O}_7$ ($\text{M}=\text{Cu}, \text{Ni}$) as a function of temperature.

factor of two. This may be due to an enhancement of the metallic density of states. There is not any significant indication of moment localization for either copper or ruthenium in these samples. Each does display a small Curie tail at low temperature, likely due to the presence of microscopic amounts of impurity spins.

Seebeck coefficients (S) for $\text{Bi}_{2-x}\text{Cu}_x\text{Ru}_2\text{O}_7$ are plotted in figure 4. (Small peaks evident in the data around 300 K are instrumental.) It can be seen that values of S for undoped $\text{Bi}_2\text{Ru}_2\text{O}_7$ are between -11 and $-4 \mu\text{V}/\text{K}$, indicating that the dominant carriers are electrons. Ten percent copper doping ($x=0.2$) increases S , though the values remain negative, between -3 and $-1 \mu\text{V}/\text{K}$. However with twenty percent ($x=0.4$) doping, the seebeck coefficients become positive, and the dominant carriers cross over to hole-like.

Resistivity data are presented in figure 5. The resistivity of undoped $\text{Bi}_2\text{Ru}_2\text{O}_7$ is largely temperature independent and on the order of $1 \text{ m}\Omega\cdot\text{cm}$, consistent with the description of a poor metal. Copper doping slightly decreases the magnitude of the resistivity but maintains a similar temperature dependence compared to the undoped sample.

B. $\text{Bi}_{2-x}\text{Ni}_x\text{Ru}_2\text{O}_7$

Magnetic susceptibility data for nickel-doped samples are shown in figure 6. The top panel plots measured susceptibility as a function of temperature. In contrast to copper doping, these samples begin to display local moment behavior as nickel is substituted. The Curie-tail at low temperature that is visible on the undoped pyrochlore becomes more pronounced with 5% ($x=0.1$) nickel doping. By 20% ($x=0.4$) nickel doping, the magnetic susceptibility scales with the Curie-Weiss equation for localized paramagnetic moments. Data from nickel-

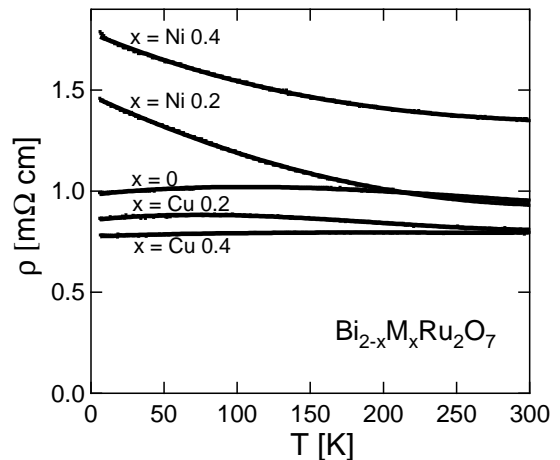


FIG. 5: Resistivity as a function of temperature for $\text{Bi}_{2-x}\text{M}_x\text{Ru}_2\text{O}_7$ ($\text{M}=\text{Cu}, \text{Ni}$).

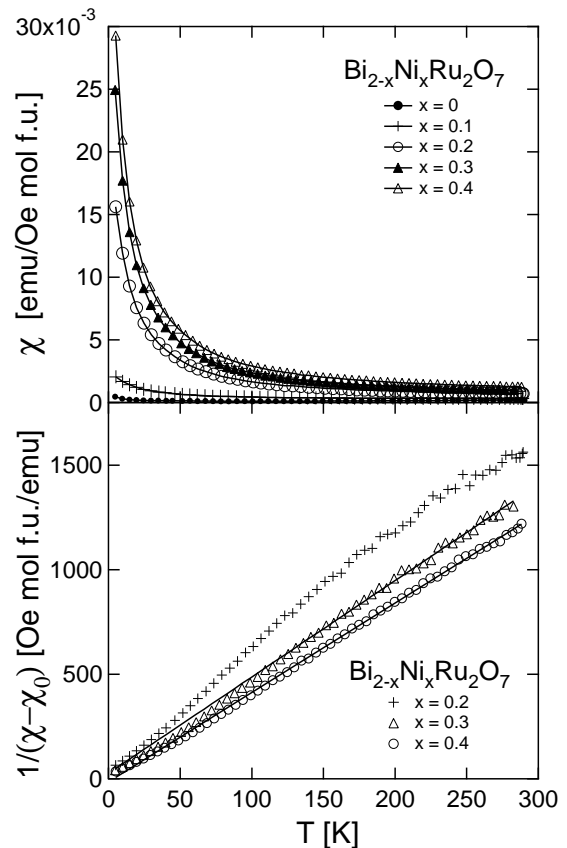


FIG. 6: Top panel: Measured magnetic susceptibility as a function of temperature for $\text{Bi}_{2-x}\text{Ni}_x\text{Ru}_2\text{O}_7$. Bottom panel: Inverse magnetic susceptibility (points) and Curie-Weiss fits (solid lines) for $\text{Bi}_{2-x}\text{Ni}_x\text{Ru}_2\text{O}_7$. Fitted temperature independent terms (χ_0) are subtracted from measured χ .

TABLE I: Calculated magnetic constants from Curie-Weiss fitting.

Dopant x	χ_0 [emu/Oe mol f.u.]	θ_{CW} [K]	μ/μ_B [per x]
Ni 0.3	2.3×10^{-4}	-4.0(9)	2.39(1)
Ni 0.4	4.4×10^{-4}	3.7(6)	2.161(3)
Co 0.1	2.2×10^{-4}	1.3(3)	4.381(4)
Co 0.2	3.8×10^{-4}	2.1(3)	4.265(4)
Co 0.3	3.8×10^{-4}	1.9(5)	4.129(4)
Co 0.4	2.5×10^{-4}	2.1(2)	4.465(2)
Co 0.5	3.0×10^{-4}	-0.7(4)	4.269(2)
Fe 0.1	3.3×10^{-4}	0.1(3)	4.937(5)
Mn 0.1	1.6×10^{-4}	1.5(4)	5.112(6)

doped samples for $x=0.3$ and $x=0.4$ were fit between 150-300 K to the function $\chi = \chi_0 + C/(T - \theta_{CW})$ where χ_0 is the sum of all temperature independent terms. Values for the effective moment and Curie-Weiss temperature (θ_{CW}) were extracted, with the results summarized in table I. Moments are between 2.1 and 2.3 μ_B/Ni , only slightly less than the theoretical spin-only value of 2.82 for Ni^{2+} . Therefore we assume that the observed local moments are accounted for by the nickel dopant, and that no local moment has been induced at ruthenium centers. Further, values of θ_{CW} are very small, indicating weak coupling between the localized spins in all cases.

The bottom panel of figure 6 plots inverse magnetic susceptibility, $1/(\chi - \chi_0)$, for the nickel-doped samples. Experimental points are overlaid by Curie-Weiss fits (solid lines) for $x=0.3$ and $x=0.4$. The overlays highlight evident deviation from ideal behavior below 100 K for the two samples. And in fact, at nickel doping levels of $x=0.2$ and lower, deviation from linear behavior is such that Curie-Weiss fitting is not applicable. Thus the magnetism can be classified as intermediate to localized and itinerant behavior.

Seebeck coefficients (S) for $\text{Bi}_{2-x}\text{Ni}_x\text{Ru}_2\text{O}_7$ are presented in figure 4. At 200 K, the magnitude of the coefficient goes from -10 in undoped $\text{Bi}_2\text{Ru}_2\text{O}_7$ to +10 $\mu\text{V}/\text{K}$ in the 10% nickel-doped sample. The nickel-doped samples have higher S values than the copper-doped samples, indicating that there is a higher concentration of hole carriers in the former. Resistivity (ρ) behavior is also different for the copper and nickel-doped samples. Figure 5 illustrates that while copper-doping decreases the magnitude of the resistivity, nickel-doping increases it. As nickel is substituted on the lattice of $\text{Bi}_2\text{Ru}_2\text{O}_7$ the resistivity becomes more like that of a degenerate semi-conductor, where ρ begins to increase slightly with decreasing temperature.

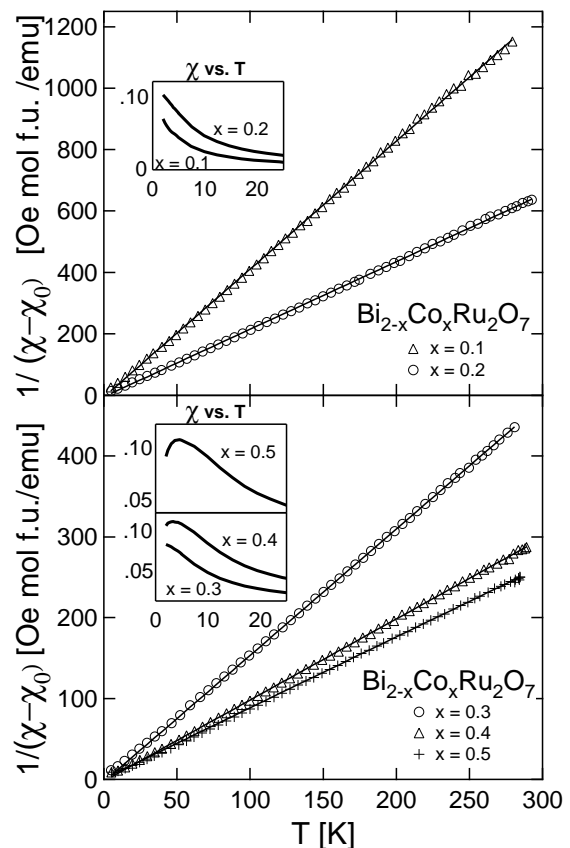


FIG. 7: Inverse magnetic susceptibility (points) and Curie-Weiss fits (solid lines) for $\text{Bi}_{2-x}\text{Co}_x\text{Ru}_2\text{O}_7$ as a function of temperature. Fitted temperature independent terms (χ_0) are subtracted from measured χ . Insets plot low temperature magnetic susceptibility down to 2 K.

C. $\text{Bi}_{2-x}\text{Co}_x\text{Ru}_2\text{O}_7$

Cobalt doping has a dramatic effect on the magnetic properties of $\text{Bi}_2\text{Ru}_2\text{O}_7$. Samples of $\text{Bi}_{2-x}\text{Co}_x\text{Ru}_2\text{O}_7$ display Curie-Weiss behavior for $x=0.1$ to 0.5 in the temperature range 300-5 K and in 1T. Plots of $1/(\chi - \chi_0)$ versus temperature (fig. 7) demonstrate the goodness of fit, where calculated values (solid lines) overlay experimental points. The effective moment normalized to cobalt content (table I) remains essentially constant across the doping series, indicating that the Curie moments are due solely to unpaired cobalt d electrons. Again no local moment is induced on ruthenium centers with doping. Calculated moments are between 4.1 and 4.4 μ_B/Co , which are slightly greater than the spin-only theoretical value of 3.87 for Co^{2+} but consistent with previously reported values for high spin Co^{2+} of 4.1 to 5.2 μ_B/Co .¹⁹ Values of theta are close to zero for all cobalt doped samples, signifying that spin-coupling is very weak. Below 5 °K, small peaks in magnetic susceptibility are observed for $x=0.4$ and $x=0.5$ samples, possibly due to spin-glass transi-

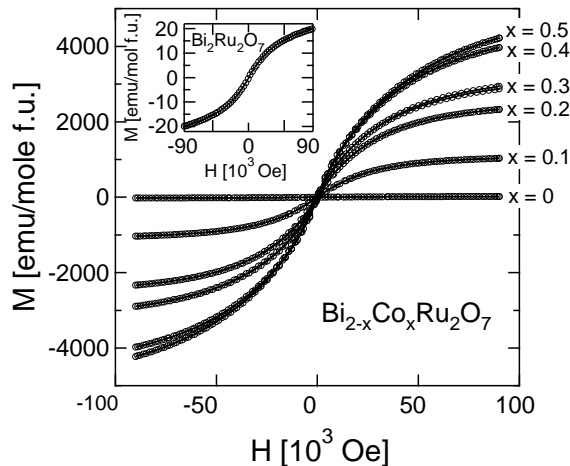


FIG. 8: Magnetization as a function of field for $\text{Bi}_{2-x}\text{Co}_x\text{Ru}_2\text{O}_7$. Inset: Expansion of measured magnetization versus field data for undoped $\text{Bi}_2\text{Ru}_2\text{O}_7$ in low temperature region. Units are: χ (emu/Oe mol f.u.), T (K).

tions (fig. 7, inset). The fact that the transitions are at such low temperatures is consistent with weak coupling of the spins. Additionally, the peak maximum increases slightly from samples $x=0.4$ to $x=0.5$. In fact, although there is not a distinct susceptibility peak for sample $x=0.3$, there are significant deviations from Curie-Weiss behavior below 5 K, signifying that some degree of interaction is present already at this doping level. The doped pyrochlores have the two characteristics common to spin-glass systems; atomic disorder and frustrated geometry.

Magnetization (M) versus field (H) curves are presented in figure 8 for $\text{Bi}_{2-x}\text{Co}_x\text{Ru}_2\text{O}_7$, where data are collected at 5 K. No magnetic hysteresis is present for any doping level. The curves are not linear, but instead scale with the paramagnetic Brillouin function, as $m\mu_B H$ is on the order of $k_B T$ at this temperature and field range. Although M vs H for undoped $\text{Bi}_2\text{Ru}_2\text{O}_7$ does appear to be flat and linear at this scale, the figure inset shows the true shape of the curve. Fitting the high field data for undoped $\text{Bi}_2\text{Ru}_2\text{O}_7$ to the Brillouin function with $g=2$, the number of localized spin 1 moments is approximated to be 0.002 spins/mol f.u. For $\text{Bi}_{2-x}\text{Co}_x\text{Ru}_2\text{O}_7$ the magnetization increases with the amount of cobalt dopant as is expected. However, attempts to fit these curves to the Brillouin function were unsuccessful. This is due to the fact that the data were collected at 5 K, where an assumption of completely localized non-interacting moments is inappropriate for these samples. Figure 9 plots magnetization as a function of H/T for sample $\text{Bi}_{1.6}\text{Co}_{0.4}\text{Ru}_2\text{O}_7$ at different temperatures. If the data follow the paramagnetic Brillouin function, then plots taken at different temperatures should superimpose. In figure 9 it is evident that plots for 25 K and 55 K data essentially overlay one another. However, data taken at 5 K deviates significantly. Therefore the

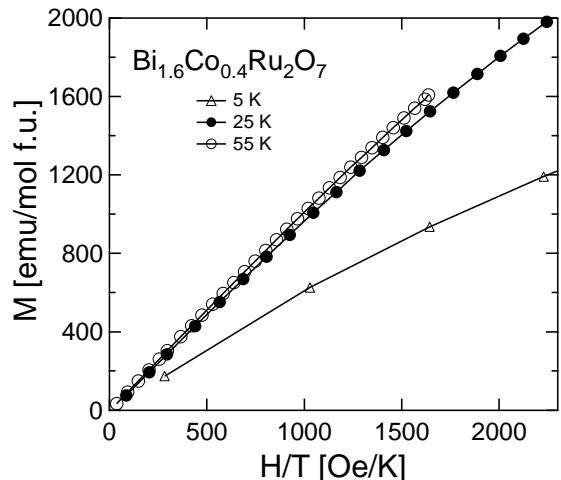


FIG. 9: Magnetization as a function of H/T for $\text{Bi}_{1.6}\text{Co}_{0.4}\text{Ru}_2\text{O}_7$, with data sets collected at three different temperatures.

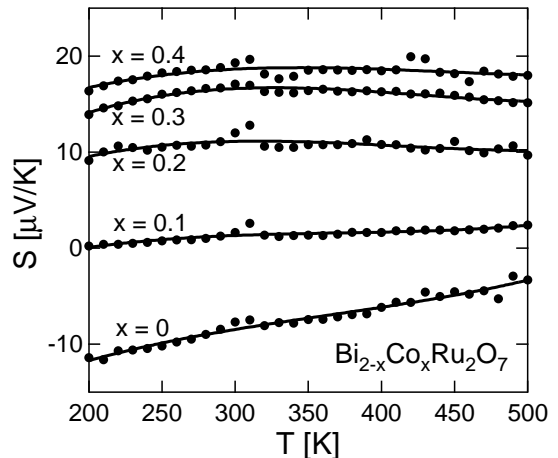


FIG. 10: Seebeck coefficients as a function of temperature for $\text{Bi}_{2-x}\text{Co}_x\text{Ru}_2\text{O}_7$.

cobalt moments are truly independent at higher temperatures, but by 5 K, some degree of interaction is present between the cobalt centers. This is supported by our susceptibility data, where possible spin-glass ordering is present below 5 K for the more heavily doped samples. It is surprising that such a large number of magnetic Co^{2+} atoms are accommodated in the pyrochlore without inducing magnetism on the ruthenium sublattice, and that the Co^{2+} spins are so weakly interacting.

Seebeck coefficients and resistivity for $\text{Bi}_{2-x}\text{Co}_x\text{Ru}_2\text{O}_7$ are plotted in figures 10 and 11 respectively. Seebeck coefficients increase with the amount of cobalt doping, reaching a maximum of $+18 \mu\text{V/K}$ for $x=0.4$. Once again, the first row transition metal is hole-doping the pyrochlore. The slope of the temperature dependence of S also becomes flatter

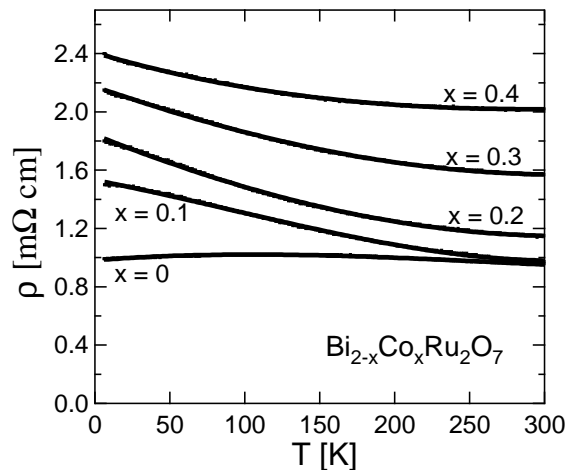


FIG. 11: Resistivity as a function of temperature for $\text{Bi}_{2-x}\text{Co}_x\text{Ru}_2\text{O}_7$.

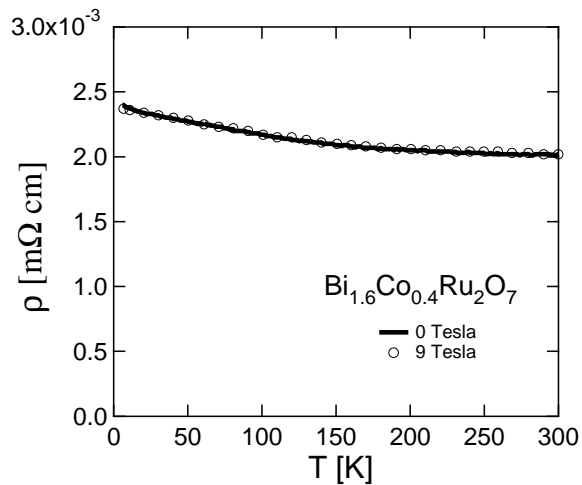


FIG. 12: Resistivity as a function of temperature for $\text{Bi}_{1.6}\text{Co}_{0.4}\text{Ru}_2\text{O}_7$ at 0 Tesla and 9 Tesla.

with increasing cobalt. The resistivity behavior of $\text{Bi}_{2-x}\text{Co}_x\text{Ru}_2\text{O}_7$ is similar to that of $\text{Bi}_{2-x}\text{Ni}_x\text{Ru}_2\text{O}_7$. As dopant is introduced, the magnitude of the resistivity increases, and the temperature dependence becomes more semi-conductor like. The increased resistivity may be due to several factors, one of which is the scattering of electrons by the localized dopant moments. This explanation is supported by the fact that in copper-doped samples, where there are no localized spins, the resistivity decreases slightly, instead of increasing. However, the resistivity of $\text{Bi}_{1.6}\text{Co}_{0.4}\text{Ru}_2\text{O}_7$ is unaffected by a field of 9T (figure 12). This is not consistent with the description of spin scattering, where at 9T the spins should align and thus decrease the resistance. Therefore the origin of resistivity behavior in copper and nickel doped $\text{Bi}_2\text{Ru}_2\text{O}_7$ is unresolved.

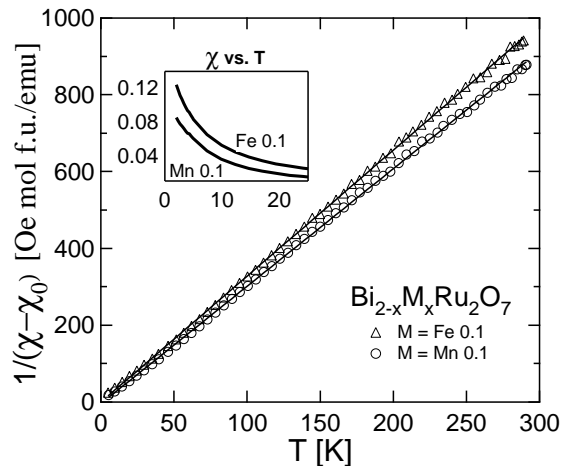


FIG. 13: Inverse susceptibility (points) and Curie-Weiss fits (solid lines) for $\text{Bi}_{1.9}\text{Mn}_{0.1}\text{Ru}_2\text{O}_7$ and $\text{Bi}_{1.9}\text{Fe}_{0.1}\text{Ru}_2\text{O}_7$ as a function of temperature. Fitted temperature independent terms (χ_0) are subtracted from measured χ . Inset plot measured magnetic susceptibility down to 2 K. Units are: χ (emu/Oe mol f.u.), T (K).

D. $\text{Bi}_{1.9}\text{Fe}_{0.1}\text{Ru}_2\text{O}_7$ and $\text{Bi}_{1.9}\text{Mn}_{0.1}\text{Ru}_2\text{O}_7$

For dopants Fe and Mn, the substitution limit is 5% ($x=0.1$). Inverse susceptibility for these two samples is plotted in figure 13, with overlaid Curie-Weiss fits (solid lines). Both $\text{Bi}_{1.9}\text{Fe}_{0.1}\text{Ru}_2\text{O}_7$ and $\text{Bi}_{1.9}\text{Mn}_{0.1}\text{Ru}_2\text{O}_7$ obey the Curie-Weiss law in the temperature range 300-5 K. Magnetic constants are listed in table I. Fitted magnetic moments are 4.9 and 5.1 μ_B/x for Fe and Mn respectively. These values are in good agreement with the spin-only theoretical value of 4.89 μ_B for $S=2$, again indicating that the observed localized moments are due to the dopants. Values of θ_{CW} are close to zero, indicating that interaction between the magnetic centers are negligible. In fact, the manganese spins are truly independent even down to low temperature. This is illustrated in figure 14, where magnetization is plotted as a function of field for $\text{Bi}_{1.9}\text{Mn}_{0.1}\text{Ru}_2\text{O}_7$. The high field data were fit to the paramagnetic Brillouin function with set values $g=2$ and $J=2$, and with only N (number of spins per mole) allowed to vary. Assuming that all localized spins originate from manganese, the resulting value of x found for $\text{Bi}_{1.9}\text{Mn}_{0.1}\text{Ru}_2\text{O}_7$ was 0.10, in agreement with the nominal concentration.

Resistivity (fig. 15) and Seebeck coefficients (fig. 16) for Mn and Fe-doped samples follow similar trends as those seen for Ni and Co. The introduction of dopant increases the magnitude of the resistivity, and samples become more semi-conducting. For Fe and Mn-doping, Seebeck coefficients also increase relative to undoped $\text{Bi}_2\text{Ru}_2\text{O}_7$ indicating that the transition metals are once again hole doping the pyrochlore.

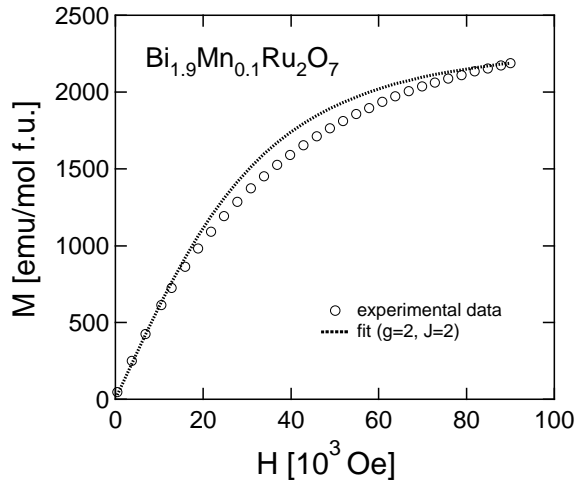


FIG. 14: Experimental magnetization vs. field data for $\text{Bi}_{1.9}\text{Mn}_{0.1}\text{Ru}_2\text{O}_7$ and paramagnetic Brillouin function (dotted line).

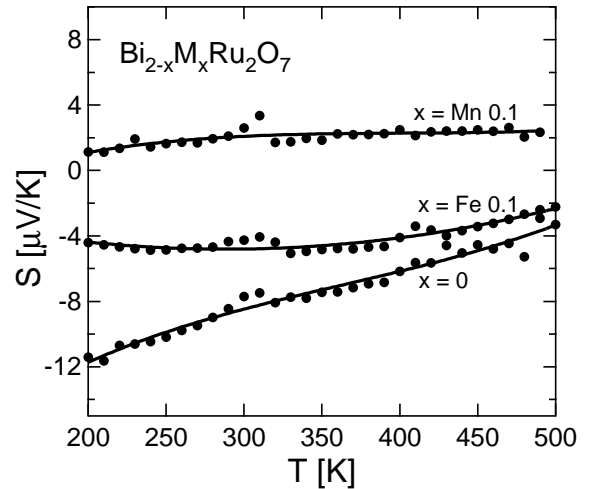


FIG. 16: Seebeck coefficient as a function of temperature for $\text{Bi}_{2-x}\text{M}_x\text{Ru}_2\text{O}_7$ ($\text{M}=\text{Fe},\text{Mn}$).

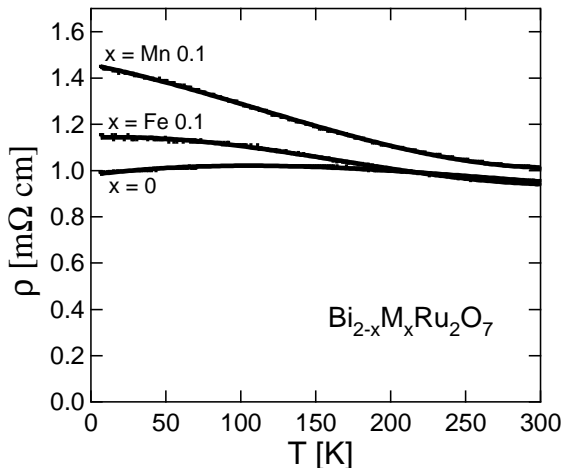


FIG. 15: Resistivity as a function of temperature for $\text{Bi}_{2-x}\text{M}_x\text{Ru}_2\text{O}_7$ ($\text{M}=\text{Fe},\text{Mn}$).

IV. DISCUSSION

The pyrochlore structure can be described as two interpenetrating networks; one of corner-sharing RuO_6 polyhedra and one of corner-sharing Bi_4O tetrahedra. Our magnetic data on transition metal doped $\text{Bi}_2\text{Ru}_2\text{O}_7$ indicates that the two networks are, surprisingly, magnetically independent.

We successfully substituted the first row transition metal series Mn^{3+} , Fe^{2+} , Co^{2+} , Ni^{2+} , and Cu^{2+} on the bismuth site of $\text{Bi}_2\text{Ru}_2\text{O}_7$. Each of these dopants has unpaired valence shell d-electrons. However, the ruthenium moments in the pyrochlore are unaffected by Bi-site doping. This is in strong contrast to results for the doped perovskites $\text{CaRu}_{1-x}\text{Ti}_x\text{O}_3$ and $\text{Sr}_2\text{Ru}_{1-x}\text{Ti}_x\text{O}_4$. Although we find no ruthenium local moments, the un-

paired dopant electrons diverge from localized to itinerant magnetic behavior across the first row transition metal series. First, in $\text{Bi}_{1.9}\text{Mn}_{0.1}\text{Ru}_2\text{O}_7$ the substituted manganese moments are localized and essentially noninteracting, even down to low temperature. In $\text{Bi}_{2-x}\text{Co}_x\text{Ru}_2\text{O}_7$ the cobalt moments are also localized, with susceptibility data fitting the Curie-Weiss law between 5-300 K. However, at low temperature the spins are no longer completely isolated. In fact, spin-glass transitions are present below 5 K for $\text{Bi}_{1.6}\text{Co}_{0.4}\text{Ru}_2\text{O}_7$ and $\text{Bi}_{1.5}\text{Co}_{0.5}\text{Ru}_2\text{O}_7$. In nickel-doped samples the unpaired nickel spins display behavior intermediate to localized and itinerant. Finally, in copper-doped samples, there is no evidence for moment localization, and only the metallic temperature independent paramagnetism is enhanced with doping. These magnetic trends are illustrated in figure 17, where the measured susceptibility at 5 K and 300 K is plotted as a function of dopant. For localized moments, the magnetic susceptibility at low temperature increases observably as a function of x, such as in the case of cobalt. However, for itinerant moments as in copper, χ_{5K} remains relatively flat with increasing x. For nickel, with atomic number intermediate to Co and Cu, the behavior is a combination of localized and itinerant. Up to $x=0.1$ χ_{5K} remains flat, while above $x=0.1$ χ_{5K} increases with x, although not as steeply as χ_{5K} in the case of cobalt. Across the series, the d-orbitals of the first row transition metal become more proximate in energy to the valance orbitals of oxygen. Thus copper hybridizes more strongly with oxygen than cobalt or nickel, resulting in itinerant behavior.

The transport properties of $\text{Bi}_{2-x}\text{M}_x\text{Ru}_2\text{O}_7$ are also evaluated. Figure 18 displays S as a function of dopant concentration for Co, Ni, and Cu doped samples. At $x=0.4$, values of S are all positive. Thus in each series the dominant carriers cross-over from electrons to holes

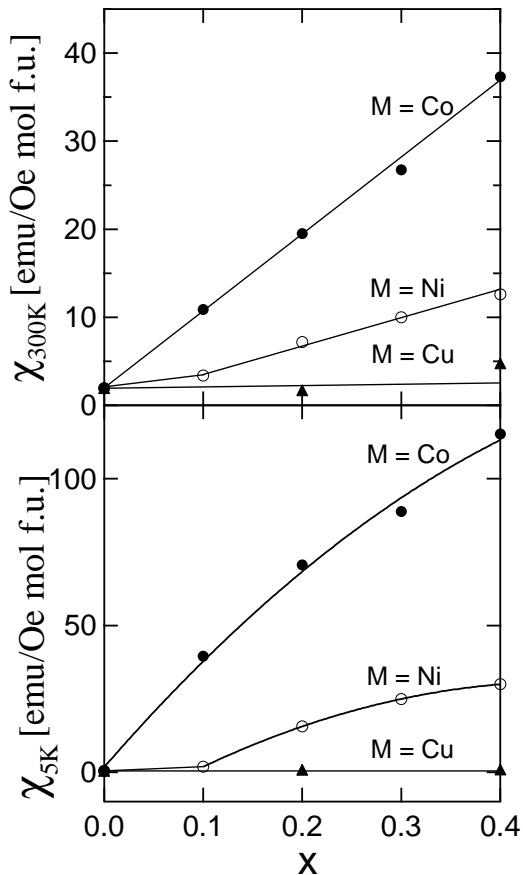


FIG. 17: Magnetic susceptibility at 300 K (top panel) and 5 K (bottom panel) as a function of dopant concentration for copper, nickel, and cobalt doped samples.

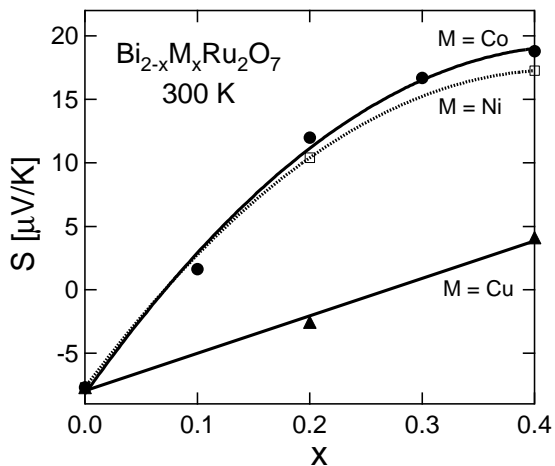


FIG. 18: Seebeck coefficients as a function of dopant concentration for copper, nickel, and cobalt doped $\text{Bi}_2\text{Ru}_2\text{O}_7$.

upon doping. The absolute value of the Seebeck coefficient, $|S|$, is proportional to $\log(N) - \log(n)$ where n is the concentration of carriers and N the available density of states. If N is essentially constant, then copper doping results in an increased concentration of carriers (n) relative to undoped $\text{Bi}_2\text{Ru}_2\text{O}_7$. This interpretation agrees with resistivity data, where the magnitude of ρ decreases as copper is substituted on the pyrochlore lattice. Conversely, Seebeck coefficients for cobalt and nickel samples increase more steeply with x than those for copper. At $x=0.4$ for these two dopants, the concentration of carriers (n) is decreased relative to undoped $\text{Bi}_2\text{Ru}_2\text{O}_7$.

V. CONCLUSION

In summary, we report magnetic and transport properties of $\text{Bi}_{2-x}\text{M}_x\text{Ru}_2\text{O}_7$ ($M=\text{Mn, Fe, Co, Ni, Cu}$). In no case did ferromagnetism or other localized ruthenium moment behavior occur upon doping. However, in such previously reported cases as $\text{CaRu}_{1-x}\text{Ti}_x\text{O}_3$ and $\text{Sr}_2\text{Ru}_{1-x}\text{Ti}_x\text{O}_4$, the dopant was substituted on the ruthenium site. Thus those substitutions could be expected to strongly perturb the Ru-O network. In the present study, the transition metal dopants preferentially replace bismuth in $\text{Bi}_2\text{Ru}_2\text{O}_7$. Our magnetic data indicates that the ruthenium and bismuth sublattices in $\text{Bi}_2\text{Ru}_2\text{O}_7$ are magnetically independent, and therefore the metal substitutions represent a second-order perturbation of the Ru-O lattice, which was not effective in causing a crossover to the ferromagnetic state. In CaRuO_3 , conversely, A-site substitution does induce ferromagnetism even though it is not a direct perturbation of the Ru-O lattice.²⁰ Therefore ruthenium oxides in the pyrochlore geometry appear to be far from the ferromagnetic instability observed in the perovskites, and such instability is not a broadly general characteristic of ruthenium oxide compounds.

Acknowledgments

This work was supported by the National Science Foundation Grant No. DMR-9808941. The work at Argonne National Laboratory was supported by the US Department of Energy, Office of Basic Energy Science, contract No. W-31-109-ENG-38.

¹ Y. Maeno, H. Hashimoto, K. Yoshida, S. Nishizaki, T. Fujita, J.G. Bednorz, and F. Lichtenberg, *Nature* **372**, 532

(1994).

- ² Y. Maeno, T.M. Rice, and M. Sigrist, *Physics Today* **54**, 42 (2001).
- ³ M. Minakata and Y. Maeno, *Phys. Rev. B* **63**, 180504 (2001).
- ⁴ K. Pucher, J. Hemberger, F. Mayr, V. Fritsch, A. Loidl, E.W. Scheidt, S. Klimm, R. Horny, S. Horn, S.G. Ebbinghaus, A. Reller, and R.J. Cava, *Phys. Rev. B* **65**, 104523 (2002).
- ⁵ S.I. Ikeda, N. Shirakawa, S. Koiwai, A. Uchida, M. Kosaka, and Y. Uwatoko, *Physica C* **364-365**, 376 (2001).
- ⁶ S.A. Grigera, R.S. Perry, A.J. Schofield, M. Chiao, S.R. Julian, G.G. Lonzarich, S.I. Ikeda, Y. Maeno, A.J. Millis, and A.P. Mackenzie, *Science* **294**, 329 (2001).
- ⁷ T. He and R.J. Cava, *J. Phys. C* **13**, 8347 (2001).
- ⁸ P.A. Cox, *Transition Metal Oxides* (Clarendon Press, Oxford, 1992).
- ⁹ B.J. Kennedy, *Physica C* **241-242**, 303 (1998).
- ¹⁰ K.S. Lee, D.K. Seo, and M.H. Whangbo, *J. Sol. St. Chem.* **131**, 405 (1997).
- ¹¹ P.A. Cox, *The Electronic Structure and Chemistry of Solids* (Clarendon Press, Oxford, 1986).
- ¹² F. Ishii and T. Oguchi, *J. Phys. Soc. Jpn.* **69**, 526 (2000).
- ¹³ W.Y. Hsu, R.V. Kasowski, T. Miller, and T.C. Chiang, *Appl. Phys. Lett.* **52**, 792 (1988).
- ¹⁴ S. Yoshii, K. Murata, and M. Sato, *Physica B* **281-282**, 619 (2000).
- ¹⁵ T. Yamamoto, R. Kanno, Y. Takeda, O. Yamamoto, Y. Kawamoto, and M. Takano, *J. Sol. St. Chem.* **109**, 372 (1994).
- ¹⁶ L. Brillouin, *J. de Phys. Radium* **8**, 74 (1927).
- ¹⁷ M. Avdeev, M.K. Haas, J.D. Jorgensen, and R.J. Cava, *J. Sol. St. Chem.*, submitted.
- ¹⁸ E. Beck and S. Kemmler-Sack, *Mat. Res. Bull.* **21**, 307 (1986).
- ¹⁹ K. Berger, *Coordination Chemistry: Experimental Methods* (Butterworth, London, 1973).
- ²⁰ T. He, Q. Huang, and R.J. Cava, *Phys. Rev. B* **63**, 024402 (2001).